

Electroplasticity Mechanisms in hcp Materials

Sebastian Herbst, Elvira Karsten, Gregory Gerstein,* Silvia Reschka, Florian Nürnberger, Stefan Zaefferer, and Hans Jürgen Maier

Herein, the mechanisms of the electroplastic effect (EPE) in different hexagonal close-packed (hcp) metals under varying loading conditions and current densities through the analysis of flow curves and microstructural changes are investigated. The investigations show a significant change in the forming behavior of the hcp materials as a result of superimposed electric current impulses. This behavior could be attributed to two effects. On the one hand, additional dislocation types are activated; on the other hand, new characteristic twin bands are formed. This is shown for all three hcp materials under investigation: Ti, Mg, and Zn. Furthermore, the hypothesis of the existence of a critical value of the current density at which a significant change in the plastic behavior occurs is verified by the experiments. The magnitude of this critical value for the analyzed hcp materials corresponds approximately to the theoretical values reported to be in the range of 1.6 to 2.0 kA mm⁻². In addition to the current density, the duration of the pulses also has an influence on the EPE. Understanding the correlation between the individual activated deformation mechanisms during electric pulse treatment can be crucial for controlling the electroplastic forming processes in a systematic and targeted manner.

1. Introduction

The application of a high-density pulse current treatment can substantially improve the deformability of metals by exploiting the electroplastic effect (EPE). The term EPE summarizes a number of different (sometimes very small) physical effects that occur simultaneously. According to the first works in the field of the EPE, this effect becomes visible as softening when the deformed material is subjected to high electric pulses (10³ to 10⁴ A mm⁻², duration of ms).^[1] It was claimed that the softening during high current impulse treatment is not the result of localized Joule heating of defects but of impulse transmission by electron wind.^[2] However, already in the work of Conrad, it was shown

that the contribution of the electron wind is clearly insufficient to explain the magnitude of the observed effect.^[3]

Microstructural investigations of the materials are necessary to develop the detailed understanding needed to fully exploit the current pulse treatment.

In principle, the EPE can be used to increase the formability of materials with low ductility and to decrease the yield strength. Thus, the use of electrical pulses during different forming processes has been investigated for many years, and a positive influence on forming operations has already been reported. For example, an improvement of the wire drawing process was reported by Gromov et al.^[4] Spizyn et al. analyzed the influence of current pulsing during rolling.^[2] The effect of high-current pulses on the flow stress in uniaxial tensile tests was analyzed by Sprecher et al.^[5] For aluminum and titanium sheets, Bach et al. analyzed the effects of current pulse treatment during

the electromagnetic forming process and found that both single and periodic pulses have a large influence on the formability.^[6] Okazaki et al. also found a significant reduction in flow stress with increasing current density.^[7–9]


The assumptions made in these publications about the possible mechanisms of the EPE have not been confirmed. In particular, a mechanism of increased fatigue strength during the current treatment was proposed.^[4] The current causes a local increase in temperature in places with discontinuities in the structure of the metal which in turn causes a decrease in the level of residual stresses and results in a stress relaxation.

The effects of softening of the material under the influence of current observed by Spizyn were explained on the basis of the electron-dislocation interaction hypothesis.^[2] It was assumed that current pulses do not lower the yield strength for reaching plasticity, but rather that discrete drops of the flow stress can be observed during plastic deformation. The stress drops increase with increasing current density. This can be explained both by the unsteady motion of dislocations along glide planes and by the breakthrough processes as dislocations move through obstacles. The dislocation structure is rearranged under the action of mechanical deformation at the moment of impulse.

Sprecher and Conrad^[5,10] noted the important role of Joule heating during current treatment. The influence of this heat and the associated change in length, which leads to a decrease in stress, cannot be neglected. For the thermally activated

S. Herbst, E. Karsten, G. Gerstein, S. Reschka, F. Nürnberger, H. J. Maier
Institut für Werkstoffkunde (Materials Science)
Leibniz University Hannover
An der Universität 2, 30823 Garbsen, Germany
E-mail: gerstein@iw.uni-hannover.de

S. Zaefferer
Department Microstructure Physics and Alloy Design
Max-Planck-Institut für Eisenforschung GmbH
Max-Planck-Straße 1, 40237 Düsseldorf, Germany

 The ORCID identification number(s) for the author(s) of this article can be found under <https://doi.org/10.1002/adem.202201912>.

DOI: 10.1002/adem.202201912

dislocation motion, the strain rate according to Conrad^[3] directly depends on: activation enthalpy, effective stress, kT (k = Boltzmann's constant, T = temperature), density of mobile dislocations, characterization of a dislocation line (Burgers vector), area of the slip plane traversed by dislocations, vibration frequency of the dislocation segment involved, Taylor factor, and activation entropy. These factors account for almost 70% of the total change in the yield stress.^[5]

Contrary to these results, it was shown that the magnitude of the stress drop can be modeled without assuming a direct interaction between the motion of electrons and dislocations.^[6] By modeling the experimental results, it was possible to explain the experimental observations only by Joule heating and thermal expansion. The assumption of a very small value of the electron-dislocation interaction was suggested.

According to ref. [11], an electric current flowing through a plastically deformed conductor changes its stress tensor and chemical potential μ . This can lead to a change in the vacancy concentration. An increase in vacancy concentration leads to an increase in dislocation climbing. However, this effect is expected to be relatively small except at high current densities.

The acceleration or deceleration of the dislocation movement depends on the direction of the electron flow with respect to the mechanical load.^[12] To date, the significance of the value of the electron-dislocation interaction of the EPE has not been determined in actual experiments.

Despite the application of advanced modeling and simulation methods based on dislocation density theory,^[13] no definite answer to the role of electron flow in the magnitude of the effect has been obtained.

It should be noted that the recent publications of the last few years contain new fundamental ideas compared to the previously expressed and unproven theories of electron-dislocation interactions, as well as new views on already published data. The development of analytical methods such as EBSD and ECCI combined with further advanced developments of modeling techniques (e.g., crystal plasticity models) enable new possibilities. For example, thermal activation models and models that take de-pinning of dislocations into account depend on electronic states and models in which dislocation motion is controlled by viscous resistance during electropulsing.^[14]

A schematic overview of the theories and mechanisms of electroplasticity (EP) and, in particular, of the non-EP electricity-related phenomena that influence the material response was recently published by Dimitrov et al.^[15] The work of Professor Hong's group has recently been significantly advanced^[16] and

considers the source of the influence of current pulses in the local redistribution of electron density on defects.

So far, determining the quantity of the electron-dislocation interaction caused by the EPE has been a rather difficult task.^[8,17] The analysis tools need to resolve the very small changes in mechanical behavior and microstructure despite the high current densities. Essentially, there are three methods to characterize the impact of the EPE. At the macro level, the influence of high electrical pulse loading during forming can be characterized by the corresponding yield curves. At the meso level, microstructural analysis of grains and grain boundaries can be carried out, and at the micro or nano level, the dislocation movement, for example in the form of a measurement of the displacement of individual dislocations, can be analyzed. Despite the fact that the latter is a very accurate method, it is rarely used due to high difficulty of the experimental procedures.^[18,19]

In metals, a change in the electron arrangement significantly affects the movement of dislocations.^[20] It is assumed that the velocity with which electrons impact dislocations has an influence on the deformability of metals.^[2,5] For verification of this assumption, a detailed description and investigation of the influence of electrons on the dislocation motion are necessary. To increase the accuracy of the microstructural analysis and facilitate this description, a significant increase of the current density or investigations at the nano-level is needed.

1.1. Crystallographically Based Selection of Metals for the Investigation

The crystallographic data on dislocation slip in the hcp metals studied are given in **Table 1**. Depending on the ratio c/a , either prismatic or basal slip along the direction a is usually the primary and dominant deformation mechanism in Mg, Ti, and Zn. These metals are characterized by easy glide in the basal plane and difficult dislocation slip along the c -axis. Only pyramidal glide with Burgers vector $\langle c + a \rangle$ and twinning contribute to the deformation of the crystals in the c -direction. Factors that influence the formation of twins are on the one hand the packing density and the packing-defect energy.^[21] The magnitude of the packing-defect energy has a significant influence on the twin formation since a larger separation width of partial dislocations increases the probability of twinning upon reaching the critical shear stress.^[22] On the other hand, the interplanar distance and c/a -ratio are other key influencing factors.^[21,23]

Table 1. Ratio of crystallographic axes and glide systems in Mg, Ti, Zn; data extracted from.^[21,26,27,56,57]

Material	Ratio of crystallographic axes/deviation from ideal ratio	Primary glide plane/direction	Secondary glide plane/direction	Additional glide plane/direction
Ti	1.588	Prismatic	Basal	Pyramidal
	-2.8%	{10 $\bar{1}$ 0} <11 $\bar{2}$ 0>	{0001} <11 $\bar{2}$ 0>	{10 $\bar{1}$ 1} <11 $\bar{2}$ 0>, {11 $\bar{2}$ 2} <11 $\bar{2}$ 3>
Mg	1.624	Basal	Prismatic	Pyramidal
	-0.6%	{0001} <11 $\bar{2}$ 0>	{10 $\bar{1}$ 0} <11 $\bar{2}$ 0>	{10 $\bar{1}$ 1} <11 $\bar{2}$ 0>, {11 $\bar{2}$ 2} <11 $\bar{2}$ 3>
Zn	1.856	Basal	Pyramidal	Prismatic
	+13.6%	{0001} <11 $\bar{2}$ 0>	{11 $\bar{2}$ 2} <11 $\bar{2}$ 3>	{10 $\bar{1}$ 0} <11 $\bar{2}$ 0>

The materials studied were selected based on the ratio of the crystallographic axes ($\gamma = c/a$), which is one of the main criteria when it comes to deformation behavior of hcp metals. The ideal ratio of the crystallographic axes $\gamma = 1.633$ leads to the highest packing density. On this basis, the following (technically pure) materials were chosen (see Table 1): 1) Titanium with $\gamma < 1.633$: The bond lengths in the basal planes are larger than in the prism planes $\{1010\}$. Therefore, gliding predominantly occurs along the $\{1010\}$ prism planes. 2) Magnesium with $\gamma \cong 1.633$: The deformation occurs mainly by basal $\{0001\} <1120>$ glide as well as by twinning $\{1012\} <1011\}$.^[24] 3) Zinc with $\gamma > 1.633$: The dominant deformation mechanism is basal glide,^[25] with additional pyramidal glide $\{1122\} <1123>$ being active.^[26,27]

1.2. Theoretical Prediction of a Threshold Value for Effective Current Densities

An intensive theoretical analysis of the interaction between the electron flow direction and the dislocation movement during mechanical loading of metals was carried out by Kravchenko et al.,^[28,29] and the effect of the electron flow on the dislocation movement was discussed. In this context, the electron subsystem of the metal was described by free electron interaction, and the dislocation movement was described by the superposition of sound waves.

To solve this problem, it is necessary to conduct a combined analysis of the kinetic equation for conducting electrons, Maxwell's equations, and the equations of motion for the material with dislocations. With this approach, the electron flux that acts on each unit length of a dislocation as it moves can be determined. The results of these calculations indicate that if the electron speed is faster than the dislocation's speed, the influence of the electron motion on the movement of the dislocation becomes significant.

To estimate a threshold value for a significant effect of the additional force from the electrons acting on the dislocations, certain assumptions were made in the past. This included theoretical considerations of thermodynamic and electric potentials, lattice resistance to dislocation motion, and the assumption that the total energy dissipated into heat in the case of a short pulse time (milliseconds) are insignificant.

Based on the actual assumptions, different values were calculated for the critical current density that is necessary to achieve a significant effect of the electron flow on the dislocation mobility. The analysis carried out by Fiks showed that the electron wind can have an influence on the nature of the dislocation movement under a high-enough current density.^[30,31] The necessary value of the nominal current density, which is required for the stimulation of the dislocation flows, was reported to be in the range of 10^3 – 10^5 A mm⁻². Later on, Troitskii specified much higher values of the threshold current density in the range of 10^5 to 10^6 A mm⁻².^[32] However, the interactions of electrons and dislocations depend on many factors including the material treated and therefore need further analysis. For instance, the effect of electron flow on dislocation mobility under electrical current pulses can either result in the formation of new Frank–Reed sources or in a decrease of the interaction energy of dislocations with the local (point) defects. The influence of the electron flow

can be divided into three effects: (i) the initially elastic deformation gets partially replaced by plastic deformation after current impulse treatment,^[32] (ii) additional dislocations with opposite sign are produced, which causes an annihilation of existing dislocations,^[33] and (iii) new twins are formed either within the grains or at grain boundaries.^[34]

In the present study, the analysis of the mechanical properties depending on current density and the microstructural analysis after deformation with and without superimposed current pulse was conducted for three different hcp materials. The nature and peculiarities of the formation of the microstructural features were studied to obtain insight into the physical effects taking place during current pulses treatments, i.e., thermal effects or the interaction of electrons with dislocations, and thus provide explanations of the observed influence on the mechanical properties.

2. Experimental Section

Pure Ti (99.75 wt%), pure Mg (99.95 wt%), and pure Zn (99.95 wt%) were selected for the investigations. The Ti and Zn samples were cut from sheets along the rolling direction; the Mg samples were taken from extruded material along the extrusion direction. Two sample sizes were used in this work: 1) In order to study the changes in the microstructure and to determine the degree of softening of the specimen under the action of an electric pulse, specimens of the size 1 mm × 2.2 mm × 3 mm were employed so that the cross-section perpendicular to the electric current and the mechanical load was 2.2 mm². According to this area, the maximum achievable current density was 1700 A mm⁻². 2) In order to investigate the current density thresholds sufficient to cause an exponential change in the stress drop curve, 0.7 mm × 0.7 mm × 1 mm specimens were used. According to their cross-sectional area, the maximum achievable current density was 3700 A mm⁻².

Since a very good electrical contact is an important condition during the experiments, the electrodes of the power supply were ground and polished by using a vibratory polisher and the contact surfaces of the samples were brought to a low roughness by careful multistep electric wire discharge cutting. In addition, the contact quality for each sample was controlled with a thermal imaging camera when performing the electroplastic impulse tests. An example of such a control is shown in **Figure 1**. The samples were subjected to a short 1 ms current pulse. In a case of a good surface finish, the thermal imaging camera revealed near uniform heating of the sample. If the contact surface was not sufficient, hot spots and even sparking were observed (see Figure 1), and the specific specimen/experiment was disregarded. For SEM analysis, the samples were ground, polished, and etched following previous works^[35] for Mg and^[36] for Zn. The Ti samples were ground using 2500 SiC-Paper, then polished with a 6 μm diamond suspension and finished by vibratory polishing using Eposal alumina suspension (Fa. QATM) and Eposil M-11 colloidal silicon dioxide (Fa. QATM) and finally etched using a solution according to Kroll.

A central aspect of the investigations was the determination of the sample temperature during the pulse application. The heating of the samples during the testing was monitored using a FLIR ThermaCam SC3000 infrared camera. The camera

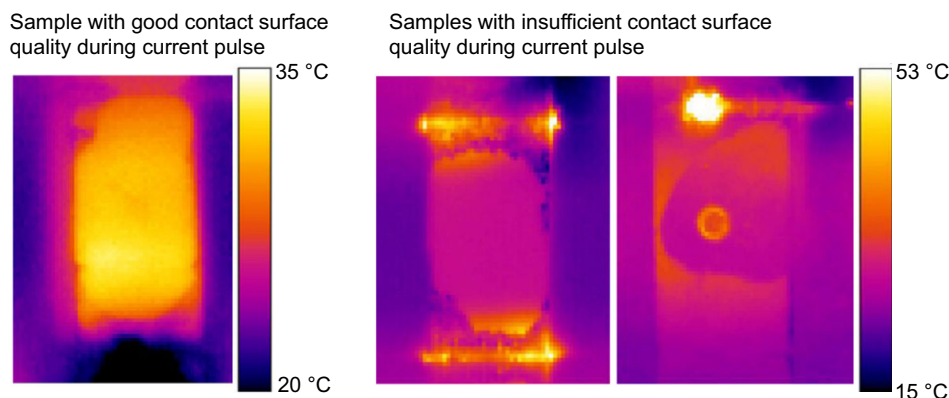


Figure 1. Heating of the sample and characterization of the quality of the contact between the sample and current supply.

had a maximum measuring frequency of 750 Hz and a thermal sensitivity of 0.02 K at 30 °C. The global specimen temperatures were also predicted using Joule's equation, cf.^[37]

For the current pulse treatment, a high current pulse generator according to refs. [33,38] was employed (see **Figure 2** left).

This system (capacitor battery of thin-film capacitors, 260 F, max. 94.5 V, charging power 0–60 V, 25 A) was chosen because a higher power output is expected in combination with high switching frequencies (high-power turn-off MOSFET, 100 × 600 A, switching capacity at 100 V, arbitrary function generator to control the MOSFET, symmetrization to avoid overvoltages). It provides a rectangular pulse of 10 μs to 100 ms with rise and fall times less than 15% of the pulse duration.

High-current pulses were applied using a Zwick universal testing machine with a constant compression rate set. Specimens were placed between the top and bottom electrodes (Figure 2, right) connected to a pulse generator. Ceramic heads were used to isolate the test machine from the current.

The samples were mounted in a universal testing machine, which was set to record a stress–strain curve, while the load

was slowly increased at a strain rate of $0.001 l_0 s^{-1}$ (l_0 : initial sample height) until 60% of the 0.2% yield strength were reached. At that point, the load increase was stopped and the electric current pulse was applied to the specimen. With this approach, the recorded stress–strain curve reliably revealed the stress drop induced by the high current pulse (schematically shown in **Figure 3**). **Table 2** summarizes the test parameters used for the different materials.

The parameters were carefully chosen to achieve the highest possible current density without heating the samples to temperatures that allow for recovery of the metals studied. Hence, $T_{\text{tests}} < 0.15 T_{\text{melting}}$ was chosen as recovery processes usually take place above $0.3 T_{\text{melting}}$.

Measurements of the temperature during the pulse loading showed that the Ti samples heated up significantly. Hence, additional compression tests were carried out on selected Ti samples in a furnace at different temperatures to quantify the thermal influence. The temperatures were selected to correspond to the sample temperature measured during the electric pulse treatments. For a current pulse duration of 0.1 ms and a current

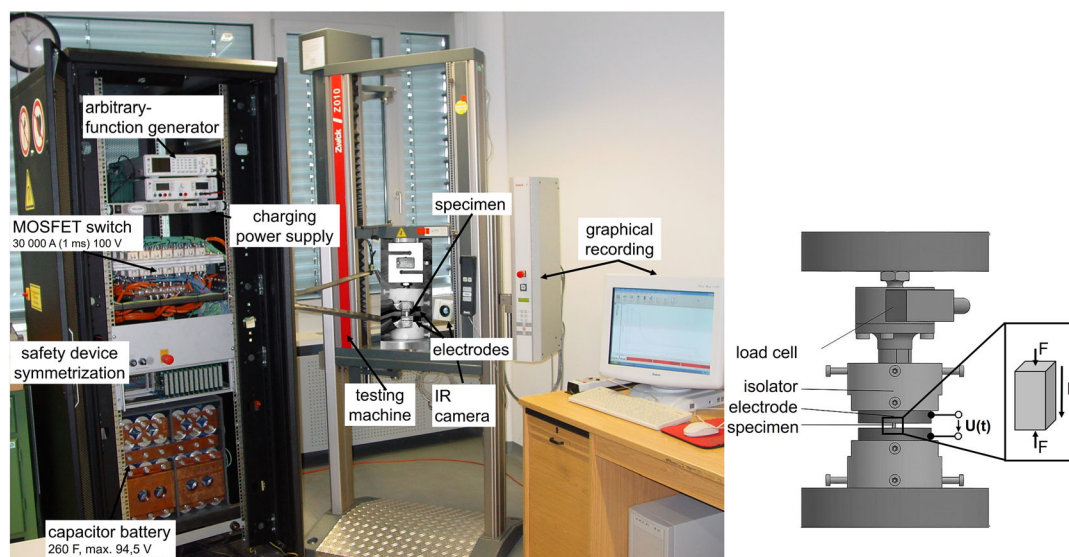


Figure 2. Set up with high current pulse generator, left and schematic representation of the experiment, right.

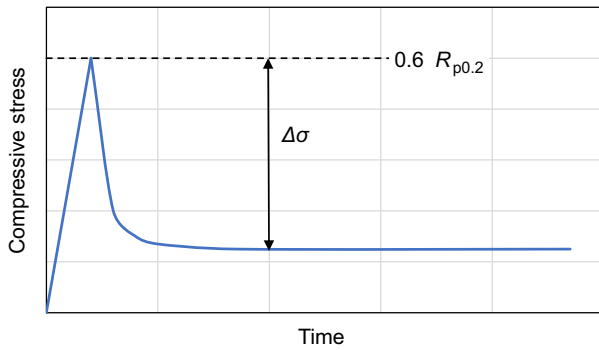


Figure 3. Schematic compressive stress–time curve (time for rise and fall of compressive stress not to scale) upon electric pulse treatments highlighting the stress drop $\Delta\sigma$ due to the electric pulse.

Table 2. Test parameters used for the different hcp materials.

Material	Electric current density J [A mm^{-2}]	Impulse duration [ms]	Mechanical load [MPa]
Mg	600–910	0.3, 0.4	25
Ti	1200–3700	0.1, 0.2	156
Zn	200–2100	0.3, 0.5	46

density of 1700 A mm^{-2} , the temperature increase corresponded to 58 K. For an initial sample temperature of $22 \text{ }^\circ\text{C}$, the peak temperature during this impulse treatment was $80 \text{ }^\circ\text{C}$. Hence, this temperature was employed for the experiments conducted within a furnace. Additional tests were carried out at $170 \text{ }^\circ\text{C}$, corresponding to a current density of 2700 A mm^{-2} . In these tests, a strain that corresponded to the strain achieved in the electric pulse experiments when the pulse was applied. This was done at 80 and $170 \text{ }^\circ\text{C}$, respectively. The measured stress was then used to calculate the corresponding stress drop due to the thermal influence.

3. Results and Discussion

3.1. Dependence of the Softening Due to EPE on Current Density

Figure 3 schematically depicts the results that were obtained from the stress–strain measurements of the compression tests with superimposed electric pulses. After reaching 60% of the 0.2% yield strength ($R_{p0.2}$), straining was stopped and the electric pulse was applied, leading to a stress drop $\Delta\sigma$.

As can be seen from Table 3, the softening of the material is different for different hcp metals. Zinc turned out to be the most sensitive to the current pulses (drop of 16 MPa at a current density of 800 A mm^{-2}), followed by magnesium (the same softening level at 1100 A mm^{-2}) and then titanium with the same softening level at 1700 A mm^{-2} . At the same time, an almost two-fold increase in current density (from 800 to 1500 A mm^{-2}) resulted in a 3.5-fold decrease in stress drop for magnesium and only a 2.5-fold decrease for zinc. A further increase of the current density up to 2100 A mm^{-2} resulted in a less steep increase in the stress drop in zinc. Correspondingly, the intense

Table 3. Variation of the stress drop of materials during the current pulse obtained during the experiments.

Material	Electric current density J [A mm^{-2}]	Stress drop $\Delta\sigma$ [MPa]
Mg	800	8
	1100	18
	1500	27
Ti	1700	18
	2100	28
	2400	38
	3700	169
Zn	800	16
	1600	39
	2100	64

stress drop in titanium is only observed at current densities much higher than 2400 A mm^{-2} .

As shown in Table 3 and the graphs in Figure 4, a similar stress drop required for deformation occurs at different current densities for different hcp metals. Therefore, in Figure 6–8, we present the results of observations of characteristic changes in twin morphology for different current densities for the corresponding hcp metals. Since for each of the metals studied the twin morphology as well as the degree of softening of the material changed at different current densities, the results are given for the corresponding current densities.

The curves in Figure 4 show an overview of the stress drop as a function of the current density based on the present study and on the results of Okazaki et al.^[7] A drop in stress was detected in all the investigated materials. The stress drop appears in Mg at the lowest current densities, followed by Zn and then Ti with the highest required current densities required. In the case of Ti, a threshold value of approximately 2200 A mm^{-2} was identified after which the stress drop increases drastically. A clearly different course of the stress drop evolution to that from the work of Okazaki et al. can be seen. This difference can be due to several reasons. On the one hand, the influence of sample size and type of the loading has a great influence on the material response. In the present study, very small samples ($0.7 \text{ mm} \times 0.7 \text{ mm} \times 1 \text{ mm}$) were used to achieve high current densities and the mechanical

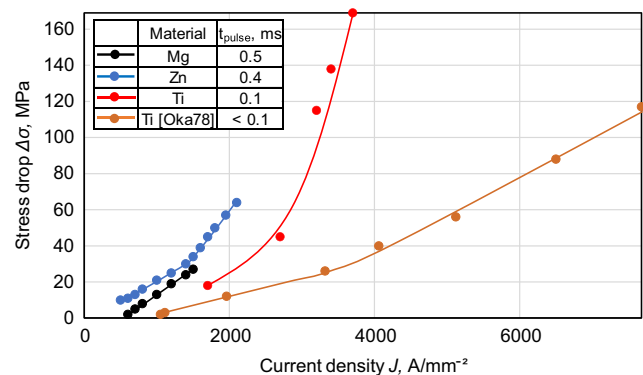


Figure 4. Influence of the electrical current density J on the stress drop $\Delta\sigma$ for Mg, Ti, and Zn.

loading was carried out in compression. Okazaki et al. employed Ti wires with a diameter of 0.12–0.51 mm, a length of 90 mm and tensile loading was applied. Another key difference appears to be stress level reached prior to the onset of the electrical pulses. In the present study, a mechanical stress well below the onset of plastic deformation was employed while Okazaki et al. applied stresses that resulted in plastic deformation prior to starting the electric pulse treatment. Finally, contact quality between the sample and the electrical power supply could be different for tension and compression loading, which in turn affects the actual specimen temperature.

Despite the mentioned factors, the overall results of the present study are in fair agreement with the results of Okazaki et al.^[7] The data obtained in present study indicate that a threshold value exists where the effect of the current pulsing becomes much more pronounced. The graph taken from Okazaki et al. also shows a bilinear course with an increased gradient at higher current densities but with a less pronounced threshold. This difference can probably be attributed to the higher initial stress (in the plastic region) applied by Okazaki et al. prior to current pulsing. The presence of the threshold value not only indicates the thermal effect by electrical current pulsing but also the electronic nature as an electron-dislocation interaction of the EPE.

A threshold value can be calculated above that the EPE causes an effective additional effect. These calculations are based on the criterion of evaluating the critical energy of the electron-dislocation interaction or the activation energy for nucleation of twins. Due to the complicated dynamics and physics of this process, some assumptions are necessary for the calculation of the threshold value: 1) The values of thermodynamic and effective electric potentials acting on free electrons as a result of local deformation of crystal lattices are equal. Correspondingly, the energy which can be absorbed or released as a result of changes in the number of the elements of the system and the interaction energy between long wavelength phonons and electrons in a solid are equal; 2) The magnitude of the critical resolved shear stress (the value of lattice resistance to dislocation motion, which determines the value of long-range internal stress fields created by dislocations and their accumulations in the plane and direction of dislocation) is in the range: 0.1–1 MPa; 3) The value of total energy dissipated into heat in the case of a short pulse flow time (milliseconds) is insignificant. (This does not mean, that the contribution of the heating effects on the EPE are insignificant).

Then, considering that the thermodynamic potential is equal to 1 eV and the value of the dissipation energy η lies in the range of 10^2 to 10^3 W cm⁻³, the calculated value of the current density for a sufficient value of the electron entrainment force of dislocations gives the value of the current density of about 1×10^3 – 3.7×10^3 A mm⁻², which correlates quite well with our results, but still requires significant specification of the calculations, taking into account the crystal-geometric and physical interaction parameters.

3.2. Thermal Influence of the Electric Current Pulses on Material Behavior

The maximum homogeneous temperature increase ΔT of a conductor due to Joule heating can be calculated with^[37]

$$\Delta T = \frac{\rho_w}{c * \rho} * J^2 * \Delta t \quad (1)$$

where J is the current density, ρ_w is the specific resistance, c is the specific heat capacity, and ρ is the density.

This of course neglects local effects like varying contact resistance or the skin effect. However, it can be employed to estimate an upper boundary for the overall heating of the bulk of the material. The material parameters of the hcp metals investigated required for the calculation of the temperature increase due to the current pulse with the current density J and the pulse duration Δt are listed in Table 4.

Figure 5 depicts the calculated correlation between current density J , current pulse duration Δt , and increase in specimen temperature ΔT for the three investigated materials. Using Ti as an example, it can be seen that with a pulse duration of 0.1 ms and a current density of 2700 A mm⁻², the theoretical sample heating is close to that of a sample loaded with a current density of 1200 A mm⁻² and a pulse duration of 0.5 ms. The temperature of the sample measured by the infrared camera matches the calculated temperature. In this case, the sample surface was covered with graphite resulting in an emissivity of 0.94. In the experiments, the duration of the current pulse and therefore the heating time of the sample is less than 1 ms and it seems possible to neglect the temperature loss during this time due to thermal conduction and convection. In the case of poor contact as a result of local heating in the contact area (Figure 1, right), the sample temperature measured by the infrared camera is higher than the calculated temperature.

During the thermal tests without pulse loading, a stress difference of 4 MPa was observed for Ti upon a temperature increase by 60 K from room temperature. This difference in

Table 4. Physical parameters of Mg, Ti, Zn employed for the calculation of Joule heating in this study.

Material	Specific resistance ρ_w [Ω mm ² mm ⁻¹]	Specific heat capacity c [J g ⁻¹ K ⁻¹]	Density ρ [g mm ⁻³]
Mg	4.6×10^{-5}	1.05	1.74×10^{-3}
Ti	47×10^{-5}	0.52	4.51×10^{-3}
Zn	6.0×10^{-5}	0.38	7.0×10^{-3}

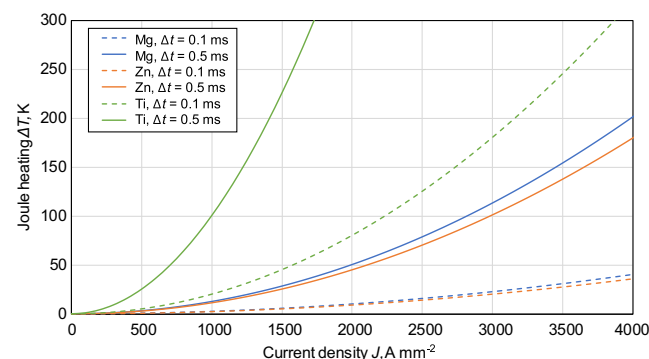


Figure 5. Calculated increase in temperature ΔT depending on current density J and pulse duration Δt in Mg, Zn, and Ti.

temperature corresponds to the heating of the sample during the current pulse of 1700 A mm^{-2} .

However, during the current pulse loading with 1700 A mm^{-2} for 0.1 ms, a stress drop of 18 MPa was measured. The measured thermal part of the stress drop (4 MPa) is therefore only 22% of the total drop of 18 MPa. Thus, the remaining 78% reflect the better ductility of the sample due to other mechanisms.

In the case of a current pulse of 2700 A mm^{-2} , an increase in the sample temperature of 150 K was measured. In the thermo-mechanical experiment without current pulse loading with a corresponding furnace temperature of 170°C (RT + 150 K), a stress drop of 22 MPa was obtained. This value is 48% of the stress drop under current pulse loading. Hence, the value $\Delta\sigma$ is again substantially influenced by the current density, i.e., the electron flow. The temperature change has a less pronounced influence on the total stress drop. This can also be seen when looking at the Figure 4 and 5 together: for Zn and a pulse duration of 0.1 ms, the calculated temperature increase is only 20 K when a current density of 1800 A mm^{-2} is applied. For Mg, the temperature increase is 10 K upon a current impulse of 910 A mm^{-2} for an impulse duration of 0.5 ms. Such a small change in temperature cannot lead to such a large decrease in voltage as was observed with the pulse treatment. The deviation between the calculated and measured temperature values, despite the fact that the equation does not take into account heat conduction, convection, and other thermal parameters, was less than 10%.

3.3. SEM Analysis of the Evolution of the Dislocation and Twin Structure

For most metals, the twins have the morphology of bands connected to grain boundaries with their opposite sides. Typical variants of such twins in annealed metals are well described by.^[39] For hexagonal metals, the morphology of twins differs slightly from that described by^[39] in proportions and configuration features of the twins. The basic description of the morphological features of nucleation and growth of twins in hcp-metals is well described in ref. [40] using zinc as an example. The form of the growing twins was described, and three types of twin boundaries were distinguished: the planar interface M, the growing part G, and the twin tip T.

As the twin spacing is a dislocation-sensitive structural parameter,^[41] changes in the twin structure were investigated to shed light on the deformation dynamics and the dislocation behavior during the current pulses. Since twinning can occur as a result of dislocation movements during plastic deformation,^[39] dislocation glide in the basal plane is a prerequisite for formation of dislocation twins. Similar to this classical twin formation, specific dislocation structures can be achieved by the current treatment to also cause twin formation. On the one hand, these dislocations are the sources for the dislocation twins; on the other hand, the increase in their density leads to a change in the width of the twin package. The influence of the dislocations is therefore not only visible as a change in dislocation density but also as a change in the twin morphology. Thus, the influence of the current pulse can be evaluated by observing the twin parameter changes without the need for the complex analysis of the dislocation structures themselves.

Model conditions for the twin nucleation are based on the splitting of a dislocation into two partial dislocations followed by the movement of one partial dislocation and the fixation of the other partial dislocation. The extension of the resulting stacking fault leads to the formation of the deformation twin. Thus, when analyzing the influence of electric current impulses on the process of plastic deformation by twinning, the influence of some mechanisms on twin nucleation has to be kept in mind: 1) dislocation annihilation in the processed metal; 2) changes in the distance between partial dislocations forming the stacking faults; 3) changes in the value of local stresses in the defect area.

The results of the SEM analysis are shown in **Figure 6–10**. It can be seen that the morphology of twins obtained in all three hcp metals as a result of conventional plastic deformation (compression tests) differs significantly when compared to the morphology of twin systems obtained under the influence of electric current pulsing. The analysis of Mg tested under electric current pulsing showed that the current treatment leads to a formation of twin bands inside the grains (Figure 6b,c), which is in good agreement with previous studies on Mg and Mg alloys.^[34,35] For Mg and Zn, the morphology of twinning is similar in the basal-pyramidal glide system. The difference between the twinning reactions is a result of the different cell parameters, the size of the Burgers vectors, and the type of the secondary glide system (see Table 1). Basal pyramidal interaction leads to the formation of dislocations, which do not lie on glide planes.^[42] The Burgers vectors of such dislocations are parallel to the twinning directions in the twin material. Dislocations of this type are immobile and can cause stress concentrations that result in secondary twinning.^[43]

In Ti, the current treatment results in formation of small twins at grain boundaries and also in floating twin bands within the grains (Figure 7). Compared to classical twins described and shown in ref. [40], the morphology of the floating twins has significant differences in planar interface M and the twin tip T. From Figure 9, it can be seen that the change in the size of the small twins is directly related to the current density, i.e., the length of the twins changes from 0.5 to $2 \mu\text{m}$ at $J = 1300 \text{ A mm}^{-2}$ (Figure 9a) to 0.5 to $10 \mu\text{m}$ at $J = 2300 \text{ A mm}^{-2}$ (Figure 9b). For Ti, the pyramidal–pyramidal interaction reactions of pyramidal dislocations result in either basal glide or fixed dislocations.^[42] Furthermore, the difference in the primary glide system also influences the type of twinning^[44] and contributes to the different twin morphology under current pulse application.

In Zn, the current treatment leads to an increased number of parallel twins (packs of twin lamellae) (Figure 8b,c). As for Mg, the twin morphology depends on the Burgers vectors and type of glide system.

Overall, there is a clear dependence of the number of twins and the nature of their configuration in the grain on the current density (Figure 6–8).

3.3.1. Development of Twin Ensembles Under Pulse Loading

The formation of specific twin structures can also be achieved by pulsed mechanical loading, and is therefore well suited for comparison with the twin morphologies observed in this work.

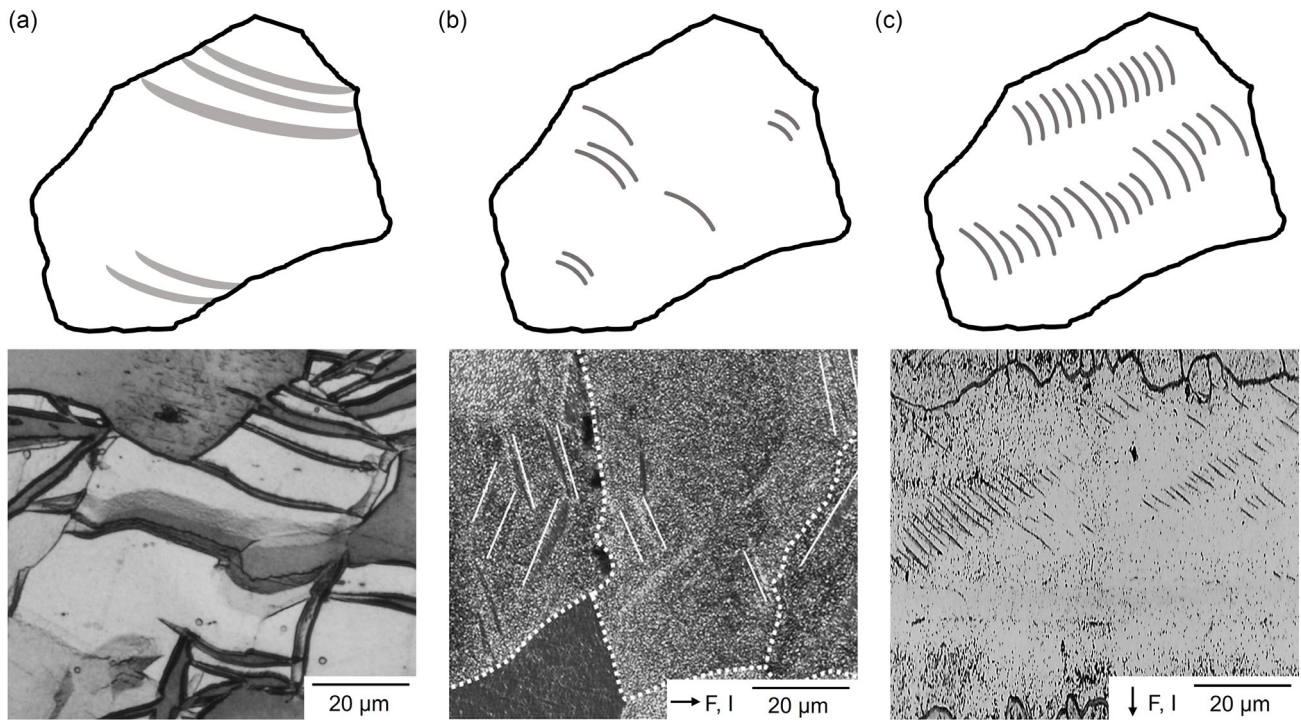


Figure 6. Twin morphologies in Mg (top: schematically, bottom: SEM micrograph): a) after conventional compression test $\epsilon = -0.01$, b) after an electro pulse of 400 A mm^{-2} for 0.3 ms, c) after an electro pulse of 800 A mm^{-2} for 0.3 ms.

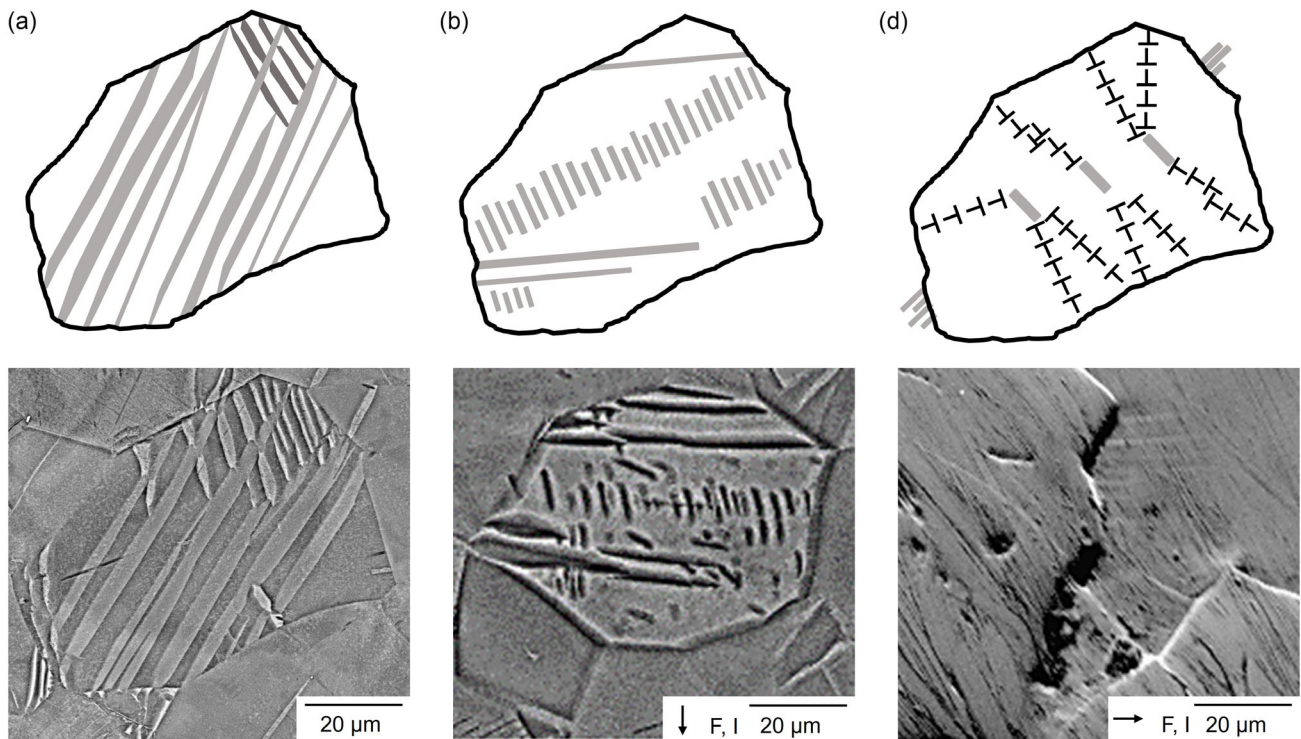


Figure 7. Twin morphologies in Ti (top: schematically, bottom: SEM micrograph): a) after conventional compression test to $\epsilon = -0.01$, b) after an electro pulse of 1700 A mm^{-2} for 0.1 ms, c) growth of dislocation walls forming low-angle boundaries conjugated with twins formed due to the electro pulse of 2400 A mm^{-2} for 0.1 ms.

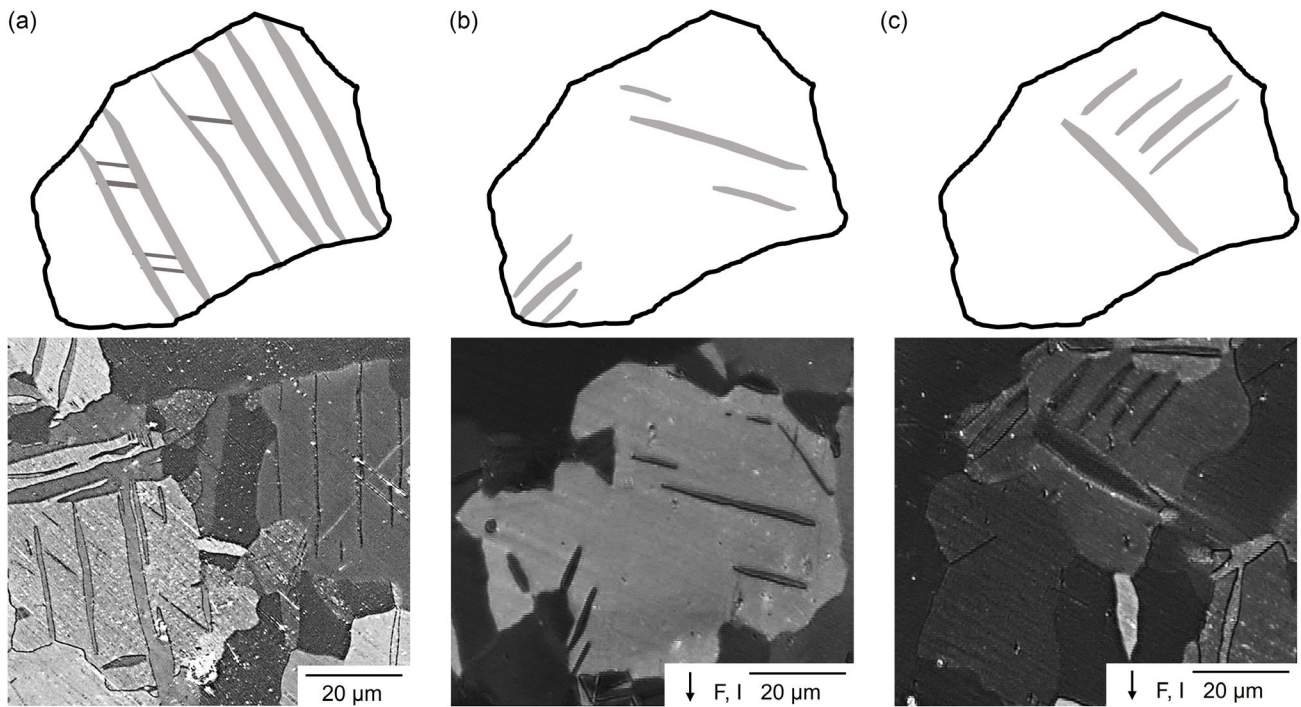


Figure 8. Twin morphologies in Zn (top: schematically, bottom: SEM micrograph): a) after conventional compression test to $\epsilon = -0.01$, b) formation of fine floating twins inside the grain, leaning or not leaning on grain boundary after an electro pulse of 910 A mm^{-2} for 0.1 ms, c) formation of coarser floating twins inside the grain, not leaning on grain boundaries after an electro pulse of 1600 A mm^{-2} for 0.1 ms.

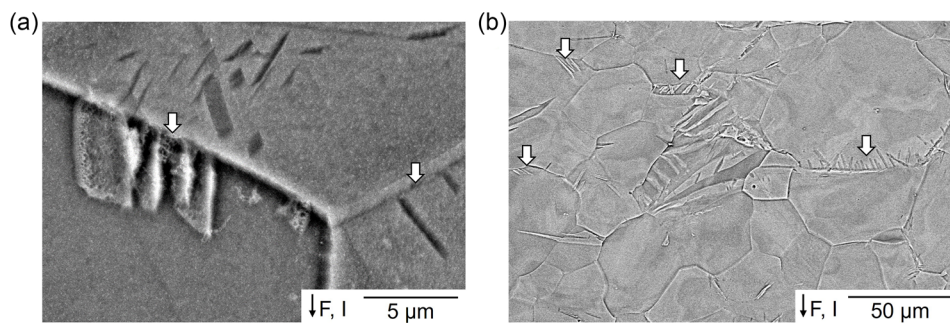


Figure 9. Morphologic details (marked by arrows) of twin growth at grain boundaries in Ti (current direction is parallel to the mechanical load direction and from top to bottom in the micrographs): a) small individual twins formed at the grain boundary after current treatment, $J = 1300 \text{ A mm}^{-2}$, for 0.1 ms, b) overview of arrangement of twins in several grains after current treatment with $J = 2300 \text{ A mm}^{-2}$, for 0.1 ms.

If we consider the current pulse as a source of electron density redistribution on defects and as a way of changing local stresses in the grain volume, then the influence of pulse deformation on nucleation, annihilation of twinning dislocations, and formation of twinning structures described in the work of the Bashmakov group^[45] is a good basis for understanding twinning processes under current pulse. In these works, it is observed that high twinning rates are achieved by pulse loading.^[45] Depending on the deformation path, twin bands of different shapes appear in the samples investigated. Under pulse loading, twins appear with parallel boundaries in the plane of cleavage and wedge shaped in the shear plane. When the twin burst stress is reached during pulse loading of the sample, the character of the twinning changes^[46] from slow development of single twins to twin burst, i.e., the

almost instantaneous occurrence in the crystal volume of a twin consisting of a large number of thin twins.^[47] It has been observed that the initial twin “burst” stress and the cleavage fracture stress are almost identical and can be represented by one straight line at all temperatures,^[48] thus the results show that the parameter kT is independent of temperature over a wide range, and provides additional support for the model of local twin nucleation along the grain boundary, similar to that discussed earlier in ref. [49] The activation energy of intense twinning for most metals is 2–4 eV.^[50] The value of this energy barrier can be significantly reduced by the work of local stresses as consideration of the real structure and geometric arrangement of dislocation piles,^[51] especially the location of dislocations in twin boundaries^[52] suggests lower values of critical stresses for twin formation.

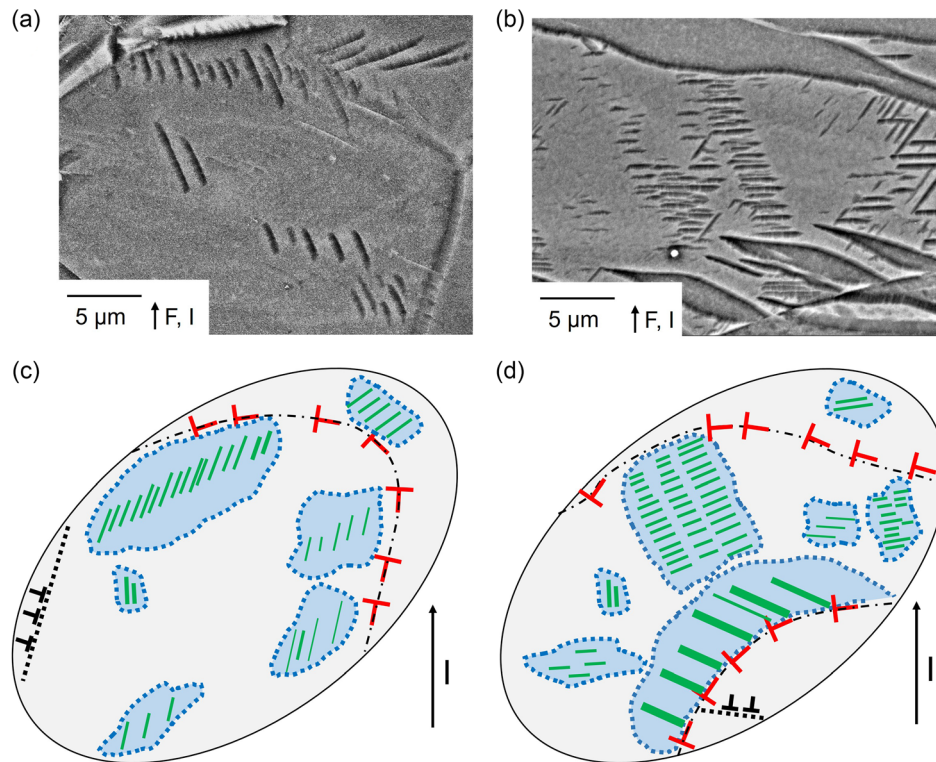


Figure 10. Laws of twin growth and twin band formation in Ti depending on current pulse density: a) growth of twins in the grain volume, $J = 1300 \text{ A mm}^{-2}$, for 0.1 ms, b) at the grain boundary, $J = 1700 \text{ A mm}^{-2}$, for 0.1 ms, c) schematic depiction showing the nucleation and growth of twins in the grain volume of (a), d) schematic depiction showing the nucleation and growth of twins in the grain volume of (b). Red dislocation symbols denote grain boundary dislocations, and black dislocation symbols denote dislocations in slip lines marked with black dashed lines. The dashed lines indicate the locations of grain boundaries. Blue areas indicate fields of charge imbalance under the influence of electric current. The green lines correspond to the newly formed twins.

The dependence of the differences in twin structure can be explained by the influence of the electron flow on the dislocation structures of the material. In Mg, Ti, and Zn, different dislocation reactions occur as a result of electron flow since these materials have different slip systems for twinning and different sizes of Burgers vectors for $\langle c + a \rangle$ dislocations. The observed morphological evolution of the twin structures is contrary to the dynamics of the twin growth in hcp metals.^[21,53] Here, the twin growth is divided into two steps: twin thickening normal to the twin plane and longitudinal growth in the other two spatial directions. This means a change of the conditions for dislocation interactions under a twin expansion is taking place. For instance, additional dislocations are formed at the twin boundaries during twin growth. Furthermore, the dislocation mobility changes, which in turn controls the twin lengthening process.^[21]

Different interactions between residual dislocation and $\langle a \rangle$ or $\langle a + c \rangle$ dislocation as well as twinning dislocations and residual dislocations or boundary dislocations and $\langle a \rangle$ or $\langle a + c \rangle$ dislocations are possible under the influence of electron current.^[54] The detected dependence of the structural changes of the twin microstructure dynamics on the dislocation configuration indicates the possibility to influence the twin structure not only by temperature but also by electron flow. If only the temperature increase had affected the twin structure during the current pulses, one would have observed a decrease in the number of twins in the volume of

the grain, which is characteristic for an increase in temperature.^[55] However, in the actual case, there is an increase of either twins or twin bands with increasing current density and pulse duration. This fact demonstrates that the effect of the current pulse is not the increase in sample temperature.

In addition, the present study shows that the microstructure evolution of metals during electrical current flow depends on the magnitude and the direction of the current flow (Figure 9). This was previously described only by.^[12] The formation and growth of small twins at the grain boundaries perpendicular to the current flow indicates local redistribution of electron density at grain boundaries during the current pulse.^[16] In ref. [16] the fundamental hypothesis of asymmetric charge distribution in the matrix material and near defects, which is caused by a sharp weakening of atomic bonding under the influence of electric current, was introduced and confirmed experimentally. For an evaluation, microstructural defects were investigated. Similar to the present study, an interdependence of twins and dislocations was found, which in turn is influenced by the electron flow during high current pulses.

Depending on the current density, the effect of the current on defects seems to occur first in the grain volume and at higher energy levels the grain boundaries are also involved (Figure 10).

The difference in size of the regions of high local stress is apparently due to the orientation of the grains and subgrains

relative to the directions of electron flow and mechanical stress, as well as to the compositional anisotropy in the sample volume. The methodology and results presented in ref. [54] help to answer important fundamental questions in the observation of twin nucleation events, namely how nanoscale twins form at boundaries or interfaces. The formation of nanoscale twin nuclei at interfaces in magnesium has been shown to indicate an intermediate step in twin development involving the nucleation and coalescence of several nuclei along the interface, occurring before the twin nucleus emerges from the interface into the crystal as a propagating lamella. Calculations based on the crystal plasticity-FFT model showed that the embryo formation is caused by local stresses generated at the twin boundary as a result of twin shear and applied external loading.

4. Conclusions

Changes in microstructural characteristics, namely twin formation, size and morphology, after electric pulse treatment with superimposed mechanical load, were analyzed for the three hcp metals Mg, Zn, and Ti. Electric current densities of up to 3700 A mm⁻² were achieved in the samples during the experiments. The main findings can be summarized as follows: 1) A large stress drop in displacement-controlled compression experiments occurs when a high electric pulse is applied. The electric pulse treatment leads to plastic deformation of the specimen, although the samples were only compressed in the elastic regime (60% of the 0.2% yield strength). 2) The magnitude of the stress drop depends on the material, the current pulse duration, and the electric current density. 3) For the materials analyzed, a threshold value of the current density was found. Above that value, the increase in stress drop with increasing current density becomes more pronounced. The presence of such a threshold value was theoretically predicted in works by other authors. 4) The increase in temperature of the specimens due to Joule heating was estimated and its influence on the mechanical properties of the material was measured. It can only explain a fraction of the observed stress drop (below 50%). Thus, the stress drop has to be mainly due to other interactions with the electric current. 5) Microstructural analyses confirmed that after electric pulse treatment, an increasing number of twins and twin bands was present compared to conventionally deformed specimens. An increased specimen temperature would have resulted in a decreased number of twins. 6) The dynamics of the changes in the morphology of the twins indicate the dislocation interaction and the processes occurring in the region of grain boundaries, defects in the structure due to electrical pulse treatment.

Acknowledgements

This work was supported by the German Research Foundation (DFG) within the Priority Program "Fields matter" (SPP 1959) under the grant number 319282412.

Conflict of Interest

The authors declare no conflict of interest.

Data Availability Statement

The data that support the findings of this study are available from the corresponding author upon reasonable request.

Keywords

electroplastic effect, high current impulses, stress drop, twinning

Received: December 29, 2022

Revised: May 15, 2023

Published online: June 23, 2023

- [1] O. A. Troitsky, *JETP Lett.* **1969**, 2, 18.
- [2] W. I. Spizyn, O. A. Troitsky, *Electroplastic Deformation of Metal*, Nauka, Moscow **1985**.
- [3] H. Conrad, *Mater. Sci. Eng.* **2002**, A322, 100.
- [4] V. E. Gromov, L. B. Zuev, E. V. Kozlov, V. J. Tsellermeier, *Electrostimulated Plasticity of Metals And Alloys*, Nedra, Moscow **1996**.
- [5] A. F. Sprecher, S. L. Mannan, H. Conrad, *Acta Metall.* **1986**, 34, 1145.
- [6] F. W. Bach, L. Walden, B. Svendsen, J. Unger, H. Blum, M. Stierner, in *Proc. of the Second Int. Conf. on High Speed Forming*, Germany, Dortmund **2006**.
- [7] K. Okazaki, M. Kagawa, H. Conrad, *Scr. Metall.* **1978**, 12, 1063.
- [8] K. Okazaki, M. Kagawa, H. Conrad, *Scr. Metall.* **1979**, 13, 473.
- [9] K. Okazaki, M. Kagawa, H. Conrad, *Mater. Sci. Eng.* **1980**, 45, 109.
- [10] H. Conrad, A. F. Sprecher, in *The Electroplastic Effect in Metals* (Eds.: F.R.N. Nabarro), Dislocations in Solids Band 8. Amsterdam, North-Holland, **1989**, p. 497.
- [11] K. M. Klimov, I. I. Novikov, *Doklady/DAN USSR* **1980**, 253, 603.
- [12] O. A. Troitsky, V. I. Likhtman, *Dokl. Akademiya Nauk SSSR* **1963**, 148, 332.
- [13] Y. Zhou, C. Wu, Z. Qu, B. Lin, *IOP Conf. Ser. Mater. Sci. Eng.*, The 19th Int. Conf. Metal. Form.(MF 2022), **2022**, 1270, 012065.
- [14] A. Lahiri, P. Shanthraj, F. Roters, *Modell. Simul. Mater. Sci. Eng.* **2019**, 27, 085006.
- [15] K. Dimitrov, Y. Liu, M. F. Horstemeyer, *Mech. Adv. Mater. Struct.* **2022**, 29, 705.
- [16] M. Kim, S. Yoon, S. Park, H. J. Jeong, J. W. Park, K. Kim, J. Jo, T. Heo, S. T. Hong, S. H. Cho, Y. K. Kwon, I. S. Choi, M. Kim, H. N. Han, *Appl. Mater. Today* **2020**, 21, 100874.
- [17] F. Nuernberger, G. Gerstein, A. Dalinger, S. E. Thuerer, A. Vinogradov, A. Feldhoff, H. J. Maier, *J. Mater. Sci.* **2017**, 52, 8007.
- [18] V. E. Gromov, T. V. Erilova, O. C. Kozhogulov, A. S. Shalpykov, *NAN KR SSR (Izv. Kirg. SSR)*, **1988**.
- [19] L. B. Zuev, V. E. Gromov, L. I. Gurevich, *Phys. Status Solidi A* **1990**, 121, 437.
- [20] V. Y. Kravchenko, *Sov. Phys. JETP* **1967**, 24, 1135.
- [21] M. H. Yoo, *Metall. Trans. A* **1981**, 12A, 409.
- [22] T. S. Byun, *Acta Mater.* **2003**, 52, 3063.
- [23] O. Cazacu, B. Plunkett, F. Barlat, *Int. J. Plast.* **2006**, 22, 1171.
- [24] A. Staroselsky, L. Anand, *Int. J. Plast.* **2003**, 19, 1843.
- [25] B. Wielke, *Acta Metall.* **1973**, 21, 289.
- [26] Y. N. Wang, J. C. Huang, *Mater. Chem. Phys.* **2003**, 81, 11.
- [27] D. J. Bacon, V. Vitek, *Metall. Mater. Trans. A* **2002**, 33A, 721.
- [28] V. Y. Kravchenko, *JETP* **1966**, 36, 1676.
- [29] V. Y. Kravchenko, *FTT* **1966**, 8, 927.
- [30] V. B. Fiks, *JETP* **1981**, 53, 790.

- [31] V. B. Fiks, *JETP* **1981**, *53*, 1209.
- [32] O. Troitsky, *Polish J. Sci.* **2021**, *38*, 39.
- [33] E. Demler, G. Gerstein, A. Dalinger, A. Epishin, T. Heidenblut, F. Nürnberger, H. J. Maier, *JMR* **2018**, *21*, 20180428.
- [34] G. Gerstein, F. Körkemeyer, A. Dalinger, S. Zaefferer, H. J. Maier, *Mater. Lett.* **2019**, *215*, 126516.
- [35] S. Reschka, G. Gerstein, A. Dalinger, S. Herbst, F. Nürnberger, S. Zaefferer, *Metallogr. Microstruct. Anal.* **2019**, *8*, 806.
- [36] H. J. Maier, E. Karsten, A. Paulsen, D. Langenkämper, P. Decker, J. Frenzel, C. Somsen, A. Ludwig, G. Eggeler, T. Niendorf, *JMR* **2017**, *23*, 4287.
- [37] D. Nuehrmann, *Das Große Werkbuch Elektronik*, Franzis-Verlag GmbH, Munich, Germany **1994**.
- [38] E. Demler, G. Gerstein, A. Dalinger, A. Epishin, D. Rodman, F. Nuernberger, *JMEPEG* **2017**, *26*, 177.
- [39] R. W. Cahn, *Adv. Phys.* **1954**, *3*, 363.
- [40] S. Lay, G. Nouet, *Philos. Mag. A* **1995**, *72*, 603.
- [41] A. M. Kosevich, V. S. Boiko, *Sov. Phys. Usp.* **1971**, *14*, 286.
- [42] V. A. Fedorov, Y. I. Tyalin, *Mashinostroenie* **2004**, *1*, 215.
- [43] F. F. Lavrentev, O. P. Salita, Y. G. Kazarov, *Phys. Meta. Metallogr.* **1968**, *26*, 348.
- [44] I. J. Beyerlein, J. Wang, M. R. Barnett, C. N. Tomé, *Proc. R. Soc. A* **2012**, *468*, 1496.
- [45] B. I. Bashmakov, T. S. Chikova, Minsk, Technoprint, **2001**, p. 218.
- [46] V. I. Bashmakov, M. E. Bosin, F. F. Lavrent'ev, I. I. Papirov, *Probl. Strength* **1974**, *1*, 80.
- [47] V. I. Bashmakov, M. E. Bosin, S. P. Shinkarenko, *Probl. Strength* **1973**, *12*, 44.
- [48] P. J. Worthington, *Scr. Metall.* **1968**, *2*, 701.
- [49] P. J. Worthington, E. Smith, *Acta Mater.* **1964**, *12*, 1277.
- [50] V. I. Vladimirov, A. N. Orlov, *Strength Mater.* **1971**, *2*, 36.
- [51] V. N. Rybin, S. K. Khannanov, *Phys. Solid State* **1969**, *11*, 1048.
- [52] V. A. Fedorov, Y. I. Tyalin, *Crystallography* **1981**, *26*, 775.
- [53] M. H. Yoo, J. K. Lee, *Philos. Mag. A* **1991**, *63*, 987.
- [54] L. Jiang, M. A. Kumar, I. J. Beyerlein, X. Wang, D. Zhang, C. Wu, C. Cooper, T. J. Rupert, S. Mahajan, E. J. Lavernia, J. M. Schoenung, *Mater. Sci. Eng. A* **2019**, *759*, 142.
- [55] G. Tsukamoto, T. Kunieda, S. Yamasaki, M. Mitsuhashi, H. Nakashima, *J. Alloys Compd.* **2021**, *884*, 161154.
- [56] T. S. Liu, M. A. Steinberg, *J. Met.* **1952**, *4*, 1043.
- [57] A. Kelly, G. W. Groves, *Crystallography and Crystal Defects*, Longman, London **1970**.